

Andrii RIABKO¹, Tetiana VAKALIUK², Oksana ZAIKA¹,
Roman KUKHARCHUK¹, Yuriy SMORZHEVSKY³

¹ Oleksandr Dovzhenko Hlukhiv National Pedagogical University, Hlukhiv, Ukraine

² Zhytomyr Polytechnic State University, Zhytomyr, Ukraine

³ Kamianets-Podilskyi Ivan Ohienko National University, Kamianets-Podilskyi, Ukraine

COMPARATIVE ANALYSIS AND SELECTION OF THE GEOMETRY OF THE MICROPHONE ARRAY BASED ON MEMS MICROPHONES FOR SOUND LOCALISATION

The **subject of this** article is the design and optimization of the geometric configuration of omnidirectional MEMS microphone arrays for sound localization tasks. The **goal** is to determine the most effective array architecture and beamforming algorithms to achieve compactness, accuracy, and balanced omnidirectional coverage. The **tasks** to be addressed include analyzing spatial-frequency characteristics of various microphone array geometries (Uniform Linear Array, Uniform Planar Array, Uniform Circular Array, and Uniform Concentric Array), comparing beamforming algorithms (delay-and-sum, differential, and superdirective), and evaluating their performance under isotropic noise fields and coherent noise sources. The **methods** used involve the application of both established and author-derived analytical models for transfer functions and directivity coefficients, as well as experimental validation using a prototype device built on a Raspberry Pi 5 platform with an Adafruit PCA9548 8-Channel STEMMMA QT expansion board and SPH0645LM4H-B omnidirectional MEMS microphones. The **results** show that similar geometric configurations of microphone arrays from omnidirectional microphones can be used for sound localization tasks at low frequencies because they are characterized by good values of Array Directivity and HPBW. This means creating a sufficiently narrow main beam, where the level of the sidelobe SLL does not differ from that of the main lobe at high frequencies. The best configurations were URA Microphone Arrays with $n = 8$ and $d = 23$ cm. **Conclusions.** Differential beamforming algorithms have demonstrated superior performance in isolation of target signals in challenging acoustic environments. The Uniform Circular Array (UCA) combined with DAS or EF DAS algorithms provides reliable omnidirectional coverage and balanced frequency response, making it ideal for applications requiring uniform sensitivity. Optimizing the spacing and radius of the microphone arrays further enhances directivity and minimizes sidelobe levels. In future work, we will focus on improving array designs using SSL reduction methods to expand localization accuracy across a wider frequency range.

Keywords: sound source localization; MEMS microphone; microphone array; directivity; beamforming algorithms.

1. Introduction

1.1. Motivation

The proliferation of smart devices, autonomous systems, and Internet of Things (IoT) technologies has created an increasing demand for accurate, reliable, and cost-effective sound localization solutions. In security and surveillance applications, there is an urgent need for systems that can accurately locate and track sound sources, particularly in urban environments where visual detection may be limited. MEMS-based solutions offer a promising approach for these applications due to their compact size and potential for distributed deployment. Industrial IoT applications increasingly require acoustic monitoring and localization capabilities for predictive

maintenance and safety systems. MEMS microphone arrays offer a practical solution for these applications due to their durability and cost-effectiveness.

Therefore, the problem of sound source localization is relevant due to the need to find cheap and effective solutions for microphone arrays. A combination of mathematical approaches such as TDOA with beamforming or the correlation method with a Kalman filter and others can be used to obtain the most accurate and stable sound source localization without using special highly sensitive equipment. In our previous research, we used an array of microphones to determine the position of an unmanned aerial vehicle (UAV) based on the sound of its engines. It was established that the localization accuracy depends on the location of the microphones. Based on the frequency dependence of direct directivity and the instability model of the microphone parameters, we developed a



method for determining the rational range of operating frequencies for the normal functioning of the microphone array. A model of a linear array of microphones based on universal MEMS microphones was proposed. This model, with a particular geometrical arrangement, forms a bidirectional pattern that can be easily converted to a one-way pattern using specialized algorithms or hardware [1].

1.2. State of the Art

Ernst et al. [2] examined the use of MEMS microphones compared to traditional condenser microphones in various aerodynamic environments, culminating in successful in-flight measurements. This study demonstrates MEMS microphones as cost-effective alternatives for high-resolution spatial measurements under challenging conditions.

In [3], the authors described MEMS microphones and highlighted their widespread use because of their low cost, high performance, and reliability. It explains the two main technologies: capacitive microphones, which use a flexible membrane and backplate to generate capacitance variations, and piezoelectric microphones, which utilize stress-induced signals in piezoelectric materials like AlN. In this section, performance and reliability testing, as well as detailed architectures, are discussed.

In paper [4], we present the development of a digital MEMS beamforming microphone array using four microphones and a Direction-of-Arrival algorithm. Testing showed 99.62% accuracy, confirming its suitability for small-scale video conferencing with up to three users and one host.

In [5], the authors proposed a piezoelectric MEMS resonant microphone array (RMA) for detecting and classifying wheezing in lung sounds. With high sensitivity ($35\text{--}265\text{ mV Pa}^{-1}$) and SNR ($79\text{--}98\text{ dBA}$) in the $200\text{--}650\text{ Hz}$ range, the RMA enhances wheezing feature distinction and improves classification accuracy using deep learning or low-power machine learning for wearable applications. In [6] explores piezoelectric MEMS microphones for IIoT devices were investigated, addressing industrial challenges such as water and dust ingress. A microphone array paired with a COTS microcontroller can discern sound direction discernment at $\leq 2000\text{ Hz}$. Testing in an anechoic chamber aligns well with theoretical models, offering proof-of-principles and open-source details for further development. In [7], the authors examined MEMS microphone array performance in distinguishing noise sources via spatial filtering, focusing on sensitivity and phase variations. A free-field method was used to evaluate these variations in 8384 Knowles SPH0641LM4H-1 microphones, revealing t-distributed histograms with $\pm 0.39\text{ dB}$ sensitivity and $\pm 0.82^\circ$ phase confidence intervals. Delay-and-sum beamforming

showed a Gumbel-distributed gain with a $-0.13/+0.10\text{ dB}$ confidence interval.

A survey of MEMS-based piezoelectric microphones covers fabrication processes, applications, and experimental methodologies. It compares materials such as AlN, ZnO, and PZT and analyzes the sensitivity, dynamic range, and challenges in thin-film growth. Future applications and advances in sensor technologies are also highlighted [8].

A 2D MEMS microphone array system for pedestrian detection operates in the $14\text{--}21\text{ kHz}$ range, offering a cost-effective, non-light-based solution for poor visibility conditions [9]. It uses FPGA and multicore processors to achieve real-time operation with beamforming, filtering, and CFAR detection algorithms. Tests confirmed reliable pedestrian detection and positioning, enabling vehicles to avoid collisions at speeds up to 50 km/h .

In [10], the authors covered MEMS-based piezoresistive and capacitive microphones, highlighting materials, transduction mechanisms, and performance factors, such as sensitivity and dynamic range. Applications of this technology span aerospace, biomedicine, and audio engineering. Emerging trends include graphene-based designs, MEMS–NEMS hybrids, AI integration, and advanced signal processing for biomedical applications.

A MEMS microphone array-based acoustic localization sensor is proposed for partial discharge (PD) detection in high-voltage equipment. The array uses eight MEMS microphones (SPV08A0LR5H-1) and features a compact, cost-effective random topology optimized through simulations [11]. The Fourier-based FFT-FISTA algorithm outperforms conventional beamforming in terms of spatial resolution and sidelobe suppression. The experimental results show an average localization error of $\sim 0.04\text{ m}$, which meets the practical application requirements.

A previous study [12] presented a cost-effective method for extending the frequency range of ultrasound MEMS microphone arrays using 3D-printed waveguides. The proposed approach reduces the acoustic aperture of the microphones, enabling a more tightly spaced microphone array layout than that possible on a printed circuit board. This technique prevents aliasing due to grating lobes, making it suitable for applications such as sound source localization and emulation of bat head-related transfer functions (HRTFs).

E. Daniel et al. introduced a 7200 MEMS microphone array ($6\text{m} \times 3\text{m}$) for aeroacoustic wind tunnel studies [13]. The array, which is composed of 800 modular panels, enables beamforming and source-directivity research. The design minimizes sidelobes and allows synchronized measurements for various aperture sizes. Tested on a $1:9.5$ scale airframe model in a wind tunnel, the system quantifies emissions and evaluates the directivity, with validation through far-field microphones.

The proposed approach enhances the wind tunnel capabilities for aeroacoustic analysis.

Z. Duanmu et al. proposed a novel acoustic-vibration capacitive MEMS microphone with a rigid diaphragm and mass blocks designed for low-frequency sound and vibration detection. The sensor features anti-stiction and hydrophobic layers for enhanced reliability and moisture resistance. The high sensitivity and low distortion make it suitable for applications like electronic stethoscopes [14].

E. Chang and colleagues used MEMS microphones in a sparse array to classify texture and estimate contact position and velocity, achieving 77.3% accuracy in texture classification. Their approach demonstrated the potential of MEMS microphones for fast tactile sensing with low error rates in localization and velocity [15].

D. Pecioski et al. proposed a low-cost MEMS microphone array for sound localization in urban environments, utilizing beamforming and distributed sensor networks to monitor noise pollution [16]. This scalable solution enables continuous acoustic data collection and real-time sound source localization across diverse urban areas.

L. Wu et al. designed dual-frequency piezoelectric MEMS microphones for wind tunnel testing to address the growing demand for compact, high-performance microphones for aeroacoustic measurements. The microphones, optimized through FEM analysis, capture pressure fluctuations and predict cabin noise excitation, with preliminary acoustic characterizations verifying their feasibility [17].

C. Cheng and collaborators developed a dynamic platform for UAV detection and tracking using a MEMS microphone array, leveraging DOA and beamforming technologies [18]. The proposed platform improves situational awareness by capturing UAV acoustic signatures, providing a robust solution for security and defense applications in challenging conditions.

Phan Le Son proposed an adaptive broadband beamforming method using a sparse, irregular microphone array designed with a simulated annealing algorithm [19]. The proposed approach maximizes distinct distances between sensors, improves sparse recovery algorithms, and includes an interpolation method for reconstructing a dense array for effective broadband beamforming.

Lei Li et al. developed the SuperSoundcompass, a miniaturized acoustic localization sensor using a seven-microphone array. The proposed system achieves high accuracy even with limited sensors. Through simulations and experiments, the proposed method demonstrated an average root-mean-square error of 1.81° at 0 dB, confirming its effectiveness under various challenging conditions [20].

Wijnings et al. found that MEMS microphone arrays can localize individual noise sources using spatial filtering, and their performance was affected by variations in microphone sensitivity and phase. This study quantifies these variations using a free-field comparison method, providing histograms for 8,384 microphones and demonstrating their effects on the gain and beamforming accuracy [21].

1.3. Objective and Approach

The main objective of this research is to develop and analyze optimal geometric configurations of MEMS microphone arrays for sound source localization.

The proposed approach involves the following steps:

1. Theoretical analysis of array geometries and beamforming algorithms.
2. Mathematical modelling of array characteristics using MATLAB.
3. Practical implementation using Raspberry Pi 5 hardware platform.
4. Performance evaluation using metrics such as Array Directivity, HPBW (Half Power Beamwidth), and SLL (Side Lobe Level).

The article is structured as follows. Section 2 presents detailed mathematical models for different beamforming approaches, analyses various array geometries, including linear, circular, and rectangular configurations, and mathematical formulations for array characteristics like directivity patterns and transfer functions. Section 3 focuses on the design and implementation of the microphone array using Raspberry Pi 5 and MEMS microphones; the comparative analysis of different array configurations using metrics like array directivity, HPBW, and SLL; and the evaluation of performance across different frequencies. Section 4 summarizes the key findings and implications.

2. Materials and research methods

After analyzing the mentioned publications, it was established that mathematical models based on the measurement of signal delays (Time Difference of Arrival, TDOA) between microphones are most often used to determine the location of the sound source using an array of microphones. Here, we consider the main approaches used to build such models.

The TDOA method determines the delay time with which sound reaches various microphones in the array. The time difference depends on the position of the sound source relative to the microphone. The source coordinates can be calculated using inverse triangulation and sound wave equations.

The TDOA formula for two microphones looks like this:

$$d = v \cdot \Delta t, \quad (1)$$

where d – distance to the sound source,

v – speed of sound (about 343 m/s in the air at temp 20°C),

Δt – the time difference between the arrival of sound waves at the microphones.

The proposed method can be extended to arrays with more microphones, thereby allowing 3D localization of the source.

The beamforming method uses the phase difference of the signals arriving at different microphones in the array to create a focused beam pattern toward the sound source. This approach allows the operator to adjust the microphone array to amplify the signal from the desired direction while suppressing noise from other directions. The mathematical model of beamforming is as follows:

$$y(t) = \sum_{i=1}^N w_i x_i(t - \tau_i), \quad (2)$$

where $y(t)$ – total output signal,

N – number of microphones,

w_i – the weight factor of each microphone,

x_i – signal from each microphone,

τ_i – delay, which is determined by taking into account the position of the microphone and the direction of the source.

The correlation method GCC-PHAT (Generalized Cross-Correlation with Phase Transform) involves calculating the correlation function for the signals of two or more microphones. Used to improve accuracy in noisy environments. GCC-PHAT calculates the cross-correlation between microphone signals, considering phase shifts, which helps to find delays between signals and localize the source:

$$R_{xy}(\tau) = F^{-1} \left(\frac{X(\hat{\omega}) Y^*(\hat{\omega})}{|X(\hat{\omega}) Y^*(\hat{\omega})|} \right), \quad (3)$$

where $R_{xy}(\tau)$ – correlation function for delay,

$X(\hat{\omega})$ i $Y(\hat{\omega})$ – Fourier images of signals,

F^{-1} – inverse Fourier transform, * – complex conjugation.

Models based on stochastic algorithms are also used for dynamic localization of the sound source, especially when moving, such as the Kalman filter, Particle Filter or Maximum Likelihood Estimation (MLE) methods. These algorithms are practical under challenging conditions — with numerous sound reflections or intense background noise. Stochastic models can use TDOA or beamforming as initial data and can adapt to changing conditions, thereby improving the real-time accuracy. Combining

several approaches, such as TDOA with beamforming or correlation with a Kalman filter, is a promising approach for creating a microphone array because it provides more accurate and stable sound localization.

Different geometries of microphone arrays are used depending on the specific tasks and signal types. Fig. 1 shows the five most common two-dimensional microphone array geometries, where each point on the XY plane corresponds to one microphone. The total number of microphones in the array is denoted as N . Classical geometries, such as circular or rectangular arrays, are simple to calculate.

Example of MATLAB code for constructing Cross Array Geometry:

```
% Cross Array Geometry parameters
N = 12; % Number of elements on each axis
L = 2; % Length of each axis (m)
% Generation of microphone positions
x_pos = linspace(-L/2, L/2, N); % Location along the X axis
y_pos = zeros(1, N); % Along the Y axis, all coordinates are 0
z_pos = zeros(1, N); % Along the Z axis, all coordinates are 0
% First line (base along X)
pos_line1 = [x_pos; y_pos; z_pos];
% Second line (base along Y)
pos_line2 = [y_pos; x_pos; z_pos];
% Combination of all positions
crossArrayPositions = [pos_line1 pos_line2];
% Normal to array elements
elNormal = zeros(2, size(crossArrayPositions, 2));
% Creating a Cross Array
crossArray = phased.ConformalArray(...
'ElementPosition', crossArrayPositions, ...
'ElementNormal', elNormal);
% Visualisation
viewArray(crossArray, 'Title', 'Cross Array Geometry');
```

There are several beamforming algorithms

- delay-and-sum (DAS);
- differential (DIF);
- superdirective beamformers (SDB).

All of them belong to models based on spatial signal processing (beamforming). There are different approaches to forming directional characteristics to localize or amplify signals.

The spatial characteristics of a microphone array are usually considered in two main noise environment scenarios: coherent and diffuse noise.

In the case of coherent noise, the main spatial characteristic is the directional diagram, which describes the level of suppression of the coherent noise depending on the direction of its arrival. In the case of diffuse noise, the leading spatial characteristic is the directivity index, which determines the average level of suppression of noise coming from all directions relative to the sound of the target source coming from the main direction.

The array can be designed to maximize noise rejection and increase sensitivity to sound from the target

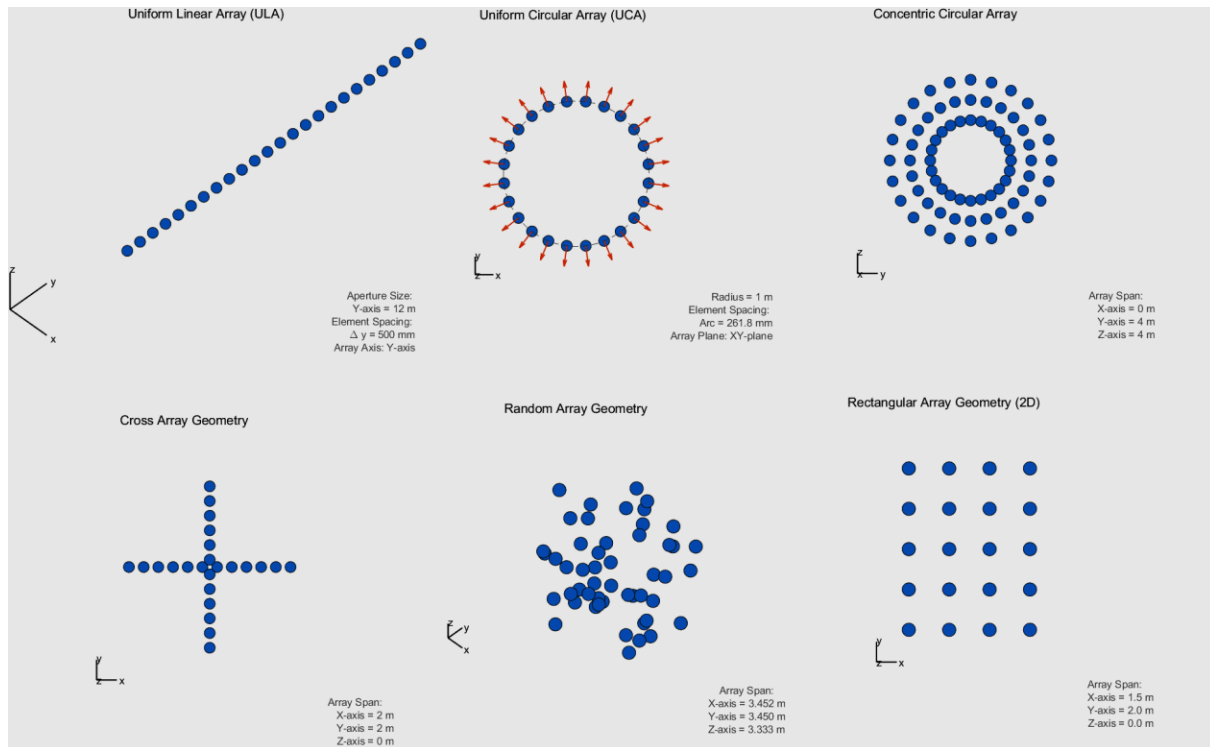


Fig. 1. 2D microphone array geometries

direction for any number of microphones. At the same time, each microphone in the array affects the formation of the directional diagram and the directional index by processing the phase and amplitude contributions of the signals. These characteristics ensure effective localization of sound even under difficult acoustic conditions.

Microphone arrays consisting of n omnidirectional microphones, spaced at a distance d from each other,

serve as the foundation for implementing beamforming algorithms such as DAS (Delay-and-Sum) and DIF (Differential) (Fig. 2).

Consider the Mathematical Model for Differential Arrays. Let us consider the properties of a microphone array with n elements that receive a signal $S(\omega, k)$ with a plane wavefront arriving from direction θ .

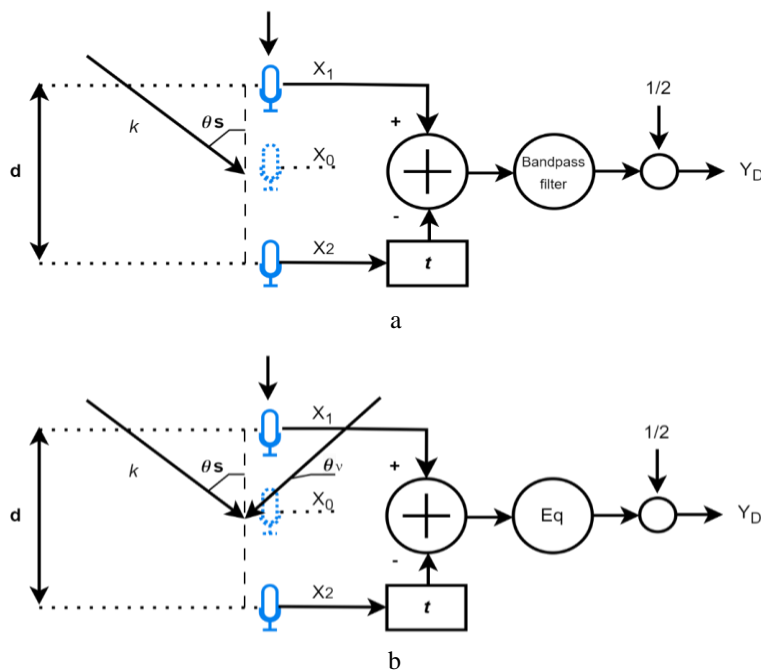


Fig. 2. Signal processing schemes of microphone arrays: with delay and summation algorithms (a); differential algorithms (b)

The time delay between signals at adjacent microphones is given by $\tau_0 = d/c$, where c is the speed of sound. In the frequency domain, the signals at the output of each microphone can be expressed as follows:

$$X_m(\omega, k) = S(\omega, k) e^{-j\omega\tau_0(m-1)\cos\theta}, \quad m=1, 2, \dots, n, \quad (4)$$

where m is the microphone index in the array.

In the DAS algorithm, the phases of the signals from all microphones are aligned according to the target signal's direction θ_s , and the signals are then summed as follows:

$$Y_{\text{DAS}}(\omega, k) = \frac{1}{n} \sum_{m=1}^n X_m(\omega, k) e^{j\omega\tau(m-1)}. \quad (5)$$

The transfer function for DAS is given as:

$$H_{\text{DAS}}(\omega, \theta) = e^{-j\frac{\omega\tau_0}{2}} \cos\left(\frac{\pi\omega\tau_0}{2}(\cos\theta - r)\right), \quad (6)$$

where $r = \frac{\tau}{\tau_0}$.

In the DIF algorithm, the phases of the signals are aligned according to the direction θ_v of the noise source, and the signals are subtracted to form a "null" in the noise direction:

$$Y_{\text{DIF}}(\omega, k) = \frac{1}{n} \sum_{m=1}^n X_m(\omega, k) e^{j\omega\tau(m-1)}. \quad (7)$$

The transfer function for DIF is given as:

$$H_{\text{DIF}}(\omega, \theta) = j e^{-j\frac{\omega\tau_0}{2}} \sin\left(\frac{\pi\omega\tau_0}{2}(r + \cos\theta)\right). \quad (8)$$

For DAS, the parameter r defines the type of directivity: Broadside (BS) ($r = 0$), endfire (EF) ($r = 1$). For DIF, the parameter r determines different types of directivity patterns: dipole ($r = 0$), hypercardioid ($r =$

0.34), supercardioid ($r = 0.57$), and cardioid ($r = 1$).

Using the transfer functions $H_{\text{DAS}}(\omega, \theta)$ and $H_{\text{DIF}}(\omega, \theta)$, the spatial and frequency properties of the microphone arrays can be analyzed to suppress noise and enhance the sensitivity to the target signal.

The spatial and frequency properties of a microphone array are described by its beampattern $B(\omega, \theta)$, which is the squared magnitude of the transfer function:

$$B(\omega, \theta) = |H(\omega, \theta)|^2. \quad (9)$$

For a microphone array with n elements, the frequency responses of the DAS and DIF algorithms exhibit distinct characteristics.

In DAS algorithms, the frequency response in the target direction θ_s is uniform and equals 1. However, if the target direction is misaligned, the frequency response becomes non-uniform, and modulation effects appear.

In DIF algorithms, the frequency response is inherently non-uniform. The response is close to zero at low frequencies, meaning that signals are suppressed. As the frequency increases, the response grows, reaching the first maximum (unity) at the cutoff frequency f_c . Beyond this point, the response oscillates between 1 and 0.

The cutoff frequency f_c is determined by the following expression:

$$f_c = \frac{1}{2}(\tau_0 + \tau) = \frac{1}{2}(\tau_0 + \tau) \frac{c}{2d(1+r)}. \quad (10)$$

The above formula shows that the operating frequency range of differential microphone arrays significantly depends on the distance between the microphones. Fig. 3 shows graphs of the DIF frequency characteristics in the target direction for different distances between the microphones.

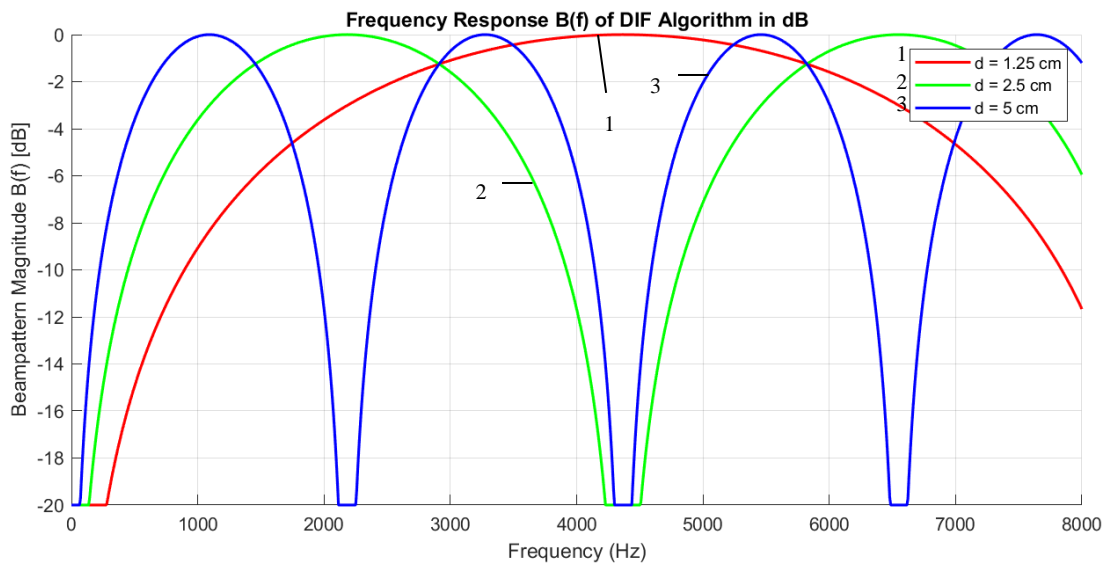


Fig. 3. Frequency response graphs of differential microphone array ($n = 2$) ($d = 1.25; 2.5; 5.0$ cm, $\theta_s = 0^\circ$, sampling frequency 16 kHz)

Let us now consider the frequency characteristics of the microphone arrays - the directivity diagram and the frequency response in the target direction $\theta = \theta_s$.

For a linear array of n microphones spaced by d , the coordinates of the k -th microphone are:

$$x_k = (k-1)d, \quad y_k = 0.$$

DAS Algorithm

$$B_{DAS}(\omega, \theta) = \left| \sum_{k=1}^n \exp \left(-j \frac{\omega}{c} ((k-1)d \cos \theta - d_s) \right) \right|^2. \quad (11)$$

where ω – angular frequency of the sound wave; c – speed of sound in the medium; θ – angle of arrival of the sound wave; d – distance between adjacent microphones in the array; d_s – delay corresponding to the target direction θ_s , given by $d_s = d \cos \theta_s$.

EF DAS Algorithm

$$B_{EF\ DAS}(\omega, \theta) = \left| \sum_{k=1}^n w_k \exp \left(-j \frac{\omega}{c} ((k-1)d \cos \theta - d_s) \right) \right|^2, \quad (12)$$

where w_k are weight coefficients.

BS DAS Algorithm

$$B_{BS\ DAS}(\omega, \theta) = \left| \sum_{k=1}^n \cos \left(\frac{\omega}{c} ((k-1)d \cos \theta - d_s) \right) \right|^2. \quad (13)$$

DIF Algorithm

$$B_{DIF}(\omega, \theta) = \left| \sum_{k=1}^n (-1)^{k-1} \exp \left(-j \frac{\omega}{c} ((k-1)d \cos \theta - d_s) \right) \right|^2. \quad (14)$$

Consider Cross Array (CA). In a cross array, microphones are arranged along two orthogonal axes.

DAS Algorithm

$$B_{DAS}(\omega, \theta) = \left| \sum_{i=1}^{n_x} \sum_{j=1}^{n_y} \exp \left(-j \frac{\omega}{c} (x_i \cos \theta + y_j \sin \theta - d_s) \right) \right|^2, \quad (15)$$

where $x_i = (i-1)d_x$ and $y_j = (j-1)d_y$;

n_x, n_y – number of microphones along the x -axis and y -axis for cross arrays;

x_k, y_k – coordinates of the k -th microphone in Cartesian coordinates.

For a Uniform Circular Array (UCA) of n microphones with radius R , the k -th microphone is located at:

$$x_k = R \cos \phi_k, \quad y_k = R \sin \phi_k, \quad \phi_k = \frac{2\pi(k-1)}{n}, \quad (16)$$

where R – radius of the circular array;

ϕ_k – angular position of the k -th microphone in a circular array.

DAS Algorithm

$$B_{DAS}(\omega, \theta) = \left| \sum_{k=1}^n \exp \left(-j \frac{\omega}{c} (R \cos(\phi_k - \theta) - d_s) \right) \right|^2. \quad (17)$$

DIF Algorithm

$$B_{DIF}(\omega, \theta) = \left| \sum_{k=1}^n (-1)^{k-1} \exp \left(-j \frac{\omega}{c} (R \cos(\phi_k - \theta) - d_s) \right) \right|^2. \quad (18)$$

In a rectangular array (RA), microphones are arranged in a grid with n_x rows and n_y columns. The coordinates of the k -th microphone are:

$$x_k = (i-1)d_x, \quad y_k = (j-1)d_y, \quad i \in \{1, \dots, n_x\}, \quad j \in \{1, \dots, n_y\}.$$

DAS Algorithm

$$B_{DAS}(\omega, \theta) = \left| \sum_{i=1}^{n_x} \sum_{j=1}^{n_y} \exp \left(-j \frac{\omega}{c} ((i-1)d_x \cos \theta + (j-1)d_y \sin \theta - d_s) \right) \right|^2. \quad (19)$$

DIF Algorithm

$$B_{DIF}(\omega, \theta) = \left| \sum_{i=1}^{n_x} \sum_{j=1}^{n_y} (-1)^{i+j} \exp \left(-j \frac{\omega}{c} ((i-1)d_x \cos \theta + (j-1)d_y \sin \theta - d_s) \right) \right|^2. \quad (20)$$

To determine the frequency characteristics of differential microphone arrays in the low-frequency range ($f \leq f_c$), an equalizer (eq) is used. For the direction $\theta_s = 0^\circ$, the equalizer has the following frequency response:

$$H_{eq}(f) = \begin{cases} \frac{1}{\sin(\pi f f_0 (r+1))}, & \text{if } f \leq f_c, \\ 1, & \text{if } f > f_c. \end{cases} \quad (21)$$

It should be noted that large values of the equalizer transfer function can lead to significant signal amplification, especially independent noise (microphone intrinsic noise, wind noise, etc.). The noise amplification degree is described by a characteristic called the White Noise Gain (WGN). Limiting the WGN value is a requirement for developing MR signal processing algorithms. A simple way to limit WGN is to limit the maximum value of the equalizer transfer function. Since the DIF directivity pattern becomes multi-lobed in the frequency range $f > 2f_c$, the operating frequency range of DIF algorithms can be limited to $2f_c$. In general, the frequency response

of a DIF with an equalizer that equalizes (without considering limitations) the response in the direction θ_s can be represented as follows:

$$B_{\text{DIF}}(\omega, \theta) = \left(\frac{\sin\left(\frac{\omega\tau_0}{2}(r+\cos\theta)\right)}{\sin\left(\frac{\omega\tau_0}{2}(r+\cos\theta_s)\right)} \right)^2. \quad (22)$$

In this case, the microphone linear array's maximum response ($n = 2$) is still located along the axis.

In a Cross Array, microphones are arranged along two orthogonal axes. The frequency response for a Cross Array can be expressed as follows:

$$B_{\text{DIF}}(\omega, \theta) = \left(\frac{\sin\left(\frac{\omega\tau_0}{2}(r_x+\cos\theta)\right) \cdot \sin\left(\frac{\omega\tau_0}{2}(r_y+\sin\theta)\right)}{\sin\left(\frac{\omega\tau_0}{2}(r_x+\cos\theta_s)\right) \cdot \sin\left(\frac{\omega\tau_0}{2}(r_y+\sin\theta_s)\right)} \right)^2, \quad (23)$$

where $r_x = \frac{x_k}{d_x}$, $r_y = \frac{y_k}{d_y}$.

In a Uniform Circular Array, microphones are uniformly distributed along a circle of radius R . The DIF frequency response for UCA is:

$$B_{\text{DIF}}(\omega, \theta) = \left(\frac{\sin\left(\frac{\omega\tau_0}{2}\left(r+\cos\theta \cdot \frac{R}{\lambda} \cos(\phi_k - \theta)\right)\right)}{\sin\left(\frac{\omega\tau_0}{2}\left(r+\cos\theta_s \cdot \frac{R}{\lambda} \cos(\phi_k - \theta_s)\right)\right)} \right)^2, \quad (24)$$

where $\phi_k = \frac{2\pi(k-1)}{n}$, $k=1, 2, \dots, n$, $r = \frac{R}{d}$;

τ_0 – time delay between adjacent microphones;

r – distance between microphones, normalised by a reference distance;

λ – wavelength of the signal;

d_x, d_y – spacing between microphones along x - and y -axes;

R – radius of the UCA;

ϕ_k – angular position of the k -th microphone in UCA.

Let us consider further the spatial characteristics of the microphone arrays.

In DAS algorithms, the time delay controls $r = \frac{\tau}{\tau_0}$ ($|r| \leq 1$) the direction of maximum sensitivity ("beam") of the microphone array $r = \cos(\theta_s)$. Taking this into account, the radiation pattern takes the following form

$$B_{\text{DAS}}(\omega, \theta) = \left| \cos\left(\frac{\omega\tau_0}{2} \cos(\theta) - \cos(\theta_s)\right) \right|^2. \quad (25)$$

This relationship shows that the maximum response of DAS linear microphone arrays is achieved in the direction $\theta = \theta_s$. Such a microphone array is called longitudinal, and the expression describes its radiation pattern:

$$B_{\text{EF}}(\omega, \theta) = \left| \cos\left(\frac{\omega\tau_0}{2} \cos(\theta) - 1\right) \right|^2. \quad (26)$$

If the direction of maximum sensitivity is close to the normal of the linear microphone arrays ($\theta_s = 90^\circ$), the microphone array is called transverse. In this case, the transfer function

$$B_{\text{EF}}(\omega, \theta) = \left(\cos\left(\frac{\omega\tau_0}{2} \cos(\theta)\right) \right)^2. \quad (27)$$

Thus, the delay value entirely determines the difference between the longitudinal and transverse microphone arrays using the DAS algorithm.

In DIF algorithms, the time delay of one of the microphone signals sets the direction $r = -\cos(\theta_v)$ of the zeros ($\pm\theta_v$) of the radiation pattern. The directivity pattern of DIF can be represented as

$$B_{\text{DIF}}(\omega, \theta) = \left| \sin\left(\frac{\omega\tau_0}{2}(r+\cos(\theta))\right) \right|^2 = \left| \sin\left(\frac{\omega\tau_0}{2}(\cos(\theta) - \cos(\theta_v))\right) \right|^2. \quad (28)$$

The frequency response of DIF with an equalizer that equalizes (without considering the limitations) the response in the direction θ_s can be represented as follows:

$$B_{\text{DIF}}(\omega, \theta) = \left(\frac{\sin\left(\frac{\omega\tau_0}{2}(\cos(\theta) - \cos(\theta_v))\right)}{\sin\left(\frac{\omega\tau_0}{2}(\cos(\theta) - \cos(\theta_v))\right)} \right)^2. \quad (29)$$

It follows from the formula that the direction of maximum sensitivity (target direction) θ_s of DIF microphone arrays always coincides with the direction of the axis. If $|\theta_v| > 90^\circ$, $\cos(\theta_v) < 0$, then $\theta_v = 0^\circ$. If $|\theta_v| < 90^\circ$, $\cos(\theta_v) > 0$, then $\theta_v = 180^\circ$. Thus, DIF microphone arrays have a longitudinal architecture, and the maximum response occurs in the hemisphere opposite to the hemisphere of zeros.

The directivity pattern describes the suppression degree (interference) of coherent signals (interference) coming from the direction θ . Coherent interference is usually formed by point sources located a short distance from the microphone array. Individual coherent interference can be suppressed by forming a zero in the direction of the interference source.

In another operating scenario, isotropic noise uniformly arrives at the microphone array from different directions. Remote or spatially distributed sources form such noise. For example, this can be the speech of third-party speakers in a room, noise in a car, or other forms of transport formed by vibration.

In these cases, the efficiency of the microphone array is characterized by the directivity factor (DF), the value of which is equal to the ratio of the response of the array in the target direction to the average response of the

array to signals coming from all directions. The following expression determines the magnitude of the directivity factor:

$$DF(\omega, \theta_s) = \frac{|H(\omega, \theta_s, \varphi_s)|^2}{\frac{1}{4\pi} \int_0^{2\pi} \int_0^\pi |H(\omega, \theta, \varphi)|^2 \sin\theta d\theta d\varphi}, \quad (30)$$

where θ_s, φ_s angles of the direction to the target source (zenith and azimuth angles, respectively).

The zenith and azimuth angles are independent. The linear microphone array radiation pattern is symmetrical about the axis; thus, the DF formula takes the following form:

$$DF(\omega, \theta_s) = \frac{|H(\omega, \theta_s)|^2}{\frac{1}{2} \int_0^\pi |H(\omega, \theta_s)|^2 \sin\theta d\theta}. \quad (31)$$

The directivity factor formulas are usually written for the direction θ_s of maximum response as $DF(\omega)$. The directivity index (DI) is calculated as the directivity coefficient in decibels:

$$DI(\omega) = 10 \log_{10} \{DF(\omega)\}. \quad (32)$$

Let us denote the power spectrum of the target signal from the direction θ_s as $P_{SS}(\omega)$ and the power spectrum of the isotropic noise coming from the surrounding space as $P_{nn}(\omega)$. The average signal-to-noise ratio (SNR) at the microphone is:

$$SNR_{in}(\omega) = 10 \log_{10} \left(\frac{P_{SS}(\omega)}{P_{nn}(\omega)} \right). \quad (33)$$

It follows that using an equalizer does not change the magnitude of the directivity factor. Considering this, the signal-to-noise ratio in decibels at the output of the

microphone array will be:

$$SNR_{out}(\omega) = SNR_{in}(\omega) + DI(\omega). \quad (34)$$

Table 1 presents the formulas for the directivity coefficient for various linear microphone array algorithms. The graphs show the directivity index for the DAS and DIF algorithms.

Table 1

Directivity coefficients of linear two-element microphone arrays

Algorithm	Directivity coefficient $DI(\omega)$
DAS	$DF(\omega, \theta_s) = \frac{1 + \cos(\omega\tau_0(\cos(\theta_s) - r))}{1 + \text{sinc}(\omega\tau_0) \cos(\omega\tau_0)}$
EF DAS	$DF(\omega, \theta_s) = \frac{2}{1 + \text{sinc}(\omega\tau_0) \cos(\omega\tau_0)}$
BS DAS	$DF(\omega, \theta_s) = \frac{2}{1 + \text{sinc}(\omega\tau_0)}$
DIF	$DF(\omega, \theta_s) = \frac{2 \left(\sin \left(\frac{\omega\tau_0}{2} (1 + r) \right) \right)^2}{1 - \text{sinc}(\omega\tau_0) \cos(\omega\tau_0)}$

The graphs (Fig. 4) show a significant directivity advantage of DIF arrays compared to DAS in the low frequency range. However, this advantage should be considered in the context of significant signal attenuation in the low frequency region.

The graphs show a significant directivity advantage of DIF arrays compared to DAS in the low frequency range. However, this advantage should be considered in the context of significant signal attenuation in the low frequency region.

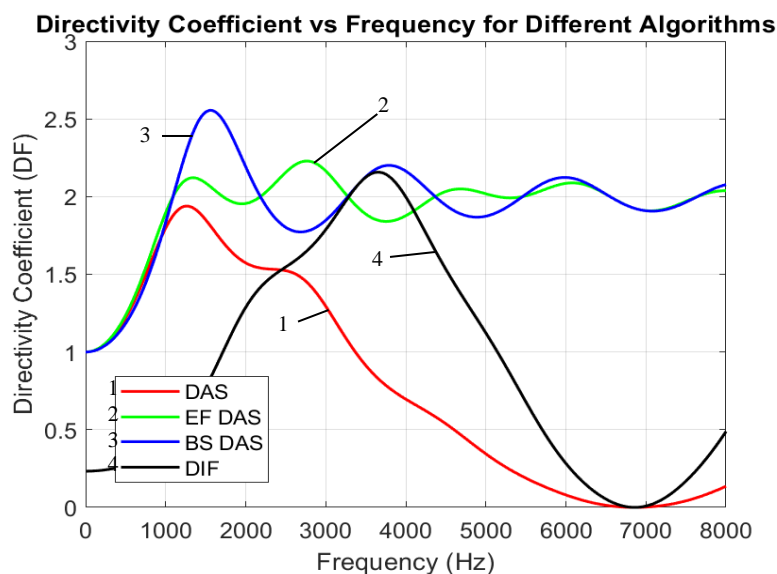


Fig. 4. Dependence of the directivity coefficient on frequency ($d = 5$ cm, sampling frequency 16 kHz)

The following tables show the directivity coefficient formulas for Cross Array (Table 2) and Uniform Circular Array (Table 3), where the symbols J_0 and J_1 represent Bessel functions of the first kind, which are solutions to Bessel's differential equation:

$$x^2 \frac{d^2 y}{dx^2} + x \frac{dy}{dx} + (x^2 - n^2)y = 0,$$

where n is an integer or an actual number,

$J_n(x)$ is the Bessel function of the first kind of order n .

$J_0(x)$ is the Bessel function of the first kind of order 0, defined as:

$$J_0(x) = \frac{1}{\pi} \int_0^\pi \cos(x \cos \theta) d\theta.$$

$J_1(x)$ is the Bessel function of the first kind of order 1, defined as:

$$J_1(x) = \frac{x}{\pi} \int_0^\pi \cos(x \cos \theta) \sin^2(\theta) d\theta.$$

The analysis of the cross-array directivity plots shows that DIF arrays outperform DAS, EF DAS, and BS DAS in terms of directivity (Fig. 5).

However, the attenuation of signals at low frequencies can negate this advantage, which limits the practical application of DIF in noisy environments. EF DAS and BS DAS in the high-frequency range showed more stable and predictable performance. DIF arrays maintain a precise directivity but can become too sensitive to phase changes, which can affect the reliability of their operation. As a result, DIF matrices provide the best low-frequency performance, sharper directivity, and better angular discrimination. BS DAS provides stable performance

at all frequencies, making it suitable for broadband microphone arrays. EF DAS provides a balance between low and high frequencies, effectively focusing energy on both frequencies. DIF arrays are recommended when low-frequency selectivity is critical, but signal attenuation must also be considered. BS DAS or EF DAS should be considered for wideband signals requiring uniform performance at all frequencies.

Table 2
Directivity coefficients for Cross Array

Algorithm	Directivity Coefficient $DI(\omega)$
DAS	$DF(\omega, \theta_s) = \frac{1 + \cos(\omega \tau_0 (\cos(\theta_s) - r))}{1 + \text{sinc}(\omega \tau_0) \cos(\omega \tau_0)}$
EF DAS	$DF(\omega, \theta_s) = \frac{2}{1 + \text{sinc}(\omega \tau_0) \cos(\omega \tau_0)}$
BS DAS	$DF(\omega, \theta_s) = \frac{2}{1 + \text{sinc}(\omega \tau_0)}$
DIF	$DF(\omega, \theta_s) = \frac{2 \sin^2\left(\frac{\omega \tau_0}{2} (1+r)\right)}{1 - \text{sinc}(\omega \tau_0) \cos(\omega \tau_0)}$

Table 3
Directivity coefficients for Uniform Circular Array

Algorithm	Directivity Coefficient $DI(\omega)$
DAS	$DF(\omega, \theta_s) = \frac{1 + J_0(\omega \tau_0)}{1 + J_1(\omega \tau_0)}$
EF DAS	$DF(\omega, \theta_s) = \frac{2}{1 + J_1(\omega \tau_0)}$
BS DAS	$DF(\omega, \theta_s) = \frac{2}{1 + J_0(\omega \tau_0)}$
DIF	$DF(\omega, \theta_s) = \frac{2 \left[\sin\left(\frac{\omega \tau_0}{2} (1+r)\right) \right]^2}{1 - J_0(\omega \tau_0)}$

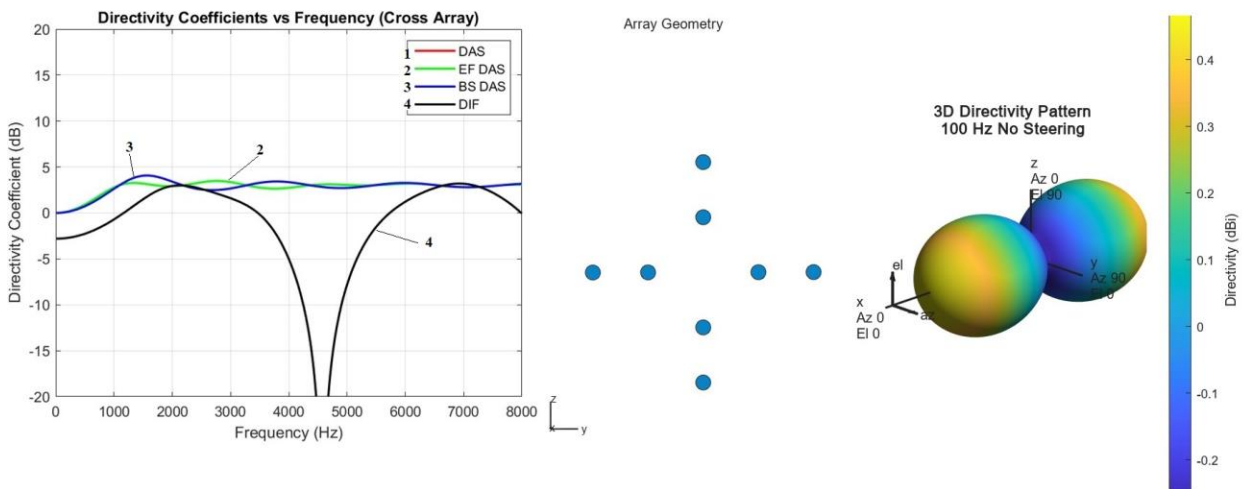


Fig. 5. Dependence of the directivity coefficient on frequency and the 3D directivity pattern ($d = 5$ cm, sampling frequency 16 kHz) for Cross Array

Before using DIF matrices in low-frequency applications, it is necessary to assess the influence of noise and environmental factors in advance.

The analysis of the Uniform Circular Array directivity plots shows that DAS and EF DAS exhibit consistent behavior, providing the same directivity coefficients (Fig. 6). BS DAS and DIF arrays exhibit reduced directivity at low frequencies, which may limit their use in such scenarios.

DIF arrays outperform other algorithms in terms of sharp angular discrimination. DAS and EF DAS maintain moderate performance, whereas the BS DAS offers stable but less discriminative responses. The oscillating nature of the Uniform Circular Array introduces variability in the directivity coefficients with increasing frequency. DIF arrays effectively exploit these variations to improve the angular resolution at higher frequencies. With this in mind, DAS is suitable for general purposes with stable frequency targeting. EF DAS is ideal for scenarios requiring energy uniformity and moderate directivity. BS DAS is recommended for applications in which the wide-area focus is more important than the angular resolution. DIF is best suited for high-frequency applications requiring precise angular selectivity, but is less effective at low frequencies.

In addition to the directivity index, other spatial characteristics were used for various scenarios of the use of a two-element microphone array:

Microphone array sensitivity ratio in the frontal and back hemispheres (Front to Back Ratio, FBR); suppression of sound from the direction opposite to the target source (Rear rejection, RR).

In the case of DIF gratings, these characteristics significantly depend on the delay parameter r . Table 4 lists the characteristics of the main differential gratings. Each microphone array specified in Table 4 has the maximum

value for one of the following criteria:

- omnidirectional microphone — the same sensitivity in all directions;
- cardioid – one zero at 180°;
- super-cardioid – maximum FBR;
- hyper cardioid – maximum DI in the low frequency range;
- dipole – maximum sensitivity at 0°/180°, the highest cutoff frequency.

One limitation of DIF gratings is the need to aim the axis of the two-element microphone array at the source of the target signal, whose position may be unknown or change during the observation process. This limitation can be partially overcome in three-element microphone arrays.

Table 4
Characteristics of differential microphone arrays

Type of microphone array (n=2)	r	DI (f = 0 Hz)	FBR	RR	Zeros	Cutoff frequency
Microphone		0 dB	1.0	0 dB	—	—
Dipole	0	4.7 dB	1.0	0 dB	±90°	1/τ ₀
Cardioid	1	4.8 dB	8.4	25 dB	180°	0.5/τ ₀
Hypercardioid	0.34	6.0 dB	8.4	6 dB	±110°	0.67/τ ₀
Supercardioid	0.57	5.7 dB	11.4	12 dB	±126°	0.78/τ ₀

The degree of directivity of the microphone array (n=2) depends on the distance between the microphones. As the distance increased, the directional pattern becomes multi-lobed (the spatial response fluctuates from zero to one). In this case, the directivity index value in DAS algorithms approaches 3 dB. Typically, the distance between microphones is limited by the following ratio:

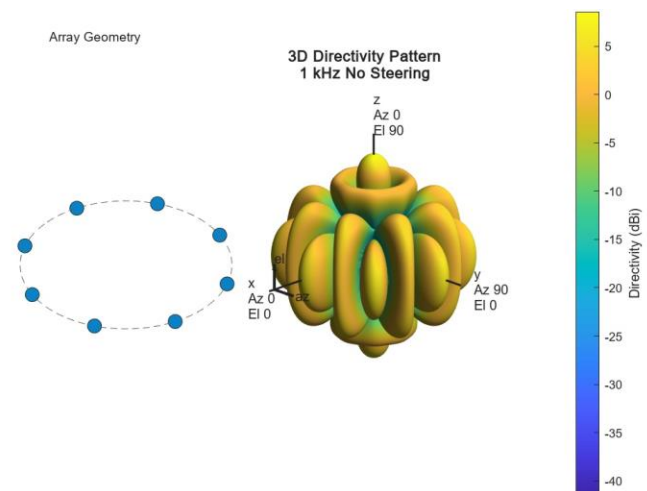
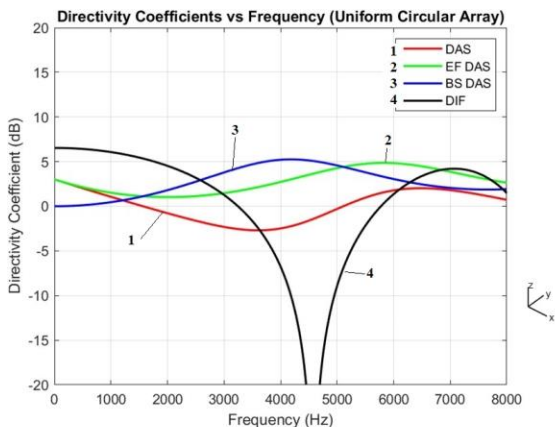


Fig. 6. Dependence of the directivity coefficient on frequency and the 3D directivity pattern (d = 5 cm, sampling frequency 16 kHz) for Uniform Circular Array

$$d \leq \frac{c}{2f_{\max}} = \frac{\lambda_{\min}}{2} \text{ or } \frac{d}{\lambda} \leq \frac{1}{2}. \quad (35)$$

The dependence of the directivity index on the ratio (d/λ) is shown in Fig. 7.

It follows from the figure and other similar calculations that the distance between the microphones, at which the maximum value of the directivity index is achieved, is minimal for the DIF algorithm and more remarkable for the DAS algorithms. In DAS algorithms, a small distance between the microphones leads to low directivity in the low-frequency range, with a slight phase shift between the microphone signals. As the distance in the high-frequency range increases, the wavelength becomes negligible compared to the distance between the microphones, the directional pattern becomes multi-lobed, and spatial leakage appears.

For DIF algorithms, a small distance between microphones corresponds to the maximum directivity of the microphone array ($n=2$) over the entire frequency range. However, small distances become problematic because they increase the sensitivity of the microphone array ($n=2$) to microphone placement errors, the spread of their characteristics, and noise.

Thus, when choosing the distance between microphones, it is necessary to ensure a compromise between high directivity over a wide frequency range and other factors. Table 5 compares the characteristics of the two-element microphone arrays.

The directivity pattern becomes more complex as the distance between the microphones increases, forming multiple lobes as the spatial response fluctuates between the minima and maxima. The directivity index (DI) of DAS algorithms in a cross array typically approaches 6 dB under ideal conditions. However, practical designs

usually limit the spacing of the array elements based on formula 35.

With the same architecture of two-element microphone arrays, different processing algorithms give them significantly different properties. Microphone arrays with differential algorithms are more compact and provide excellent noise suppression in the low-frequency range than those with delay and summation algorithms.

Table 5

Comparison of microphone arrays ($n=2$) with transverse and longitudinal architecture

Array	Advantages	Disadvantages
Broad-side DAS	flat geometry; ability to control beam direction	less suppression off-axis of the array; short distance between microphones and a large number of them are necessary to prevent spatial leakage
Endfire DAS	better off-axis rejection than Broadside; smaller overall size than Broadside	non-planar (volumetric) geometry; the direction to the source of the target signal must coincide with the axis of the array
DIF	better low frequency directivity; better off-axis rejection; smaller overall size	non-planar (volumetric) geometry; direction to the source of the useful signal must coincide with the axis of the array; more complex processing (equalizer); suppression of the target signal in the low-frequency range

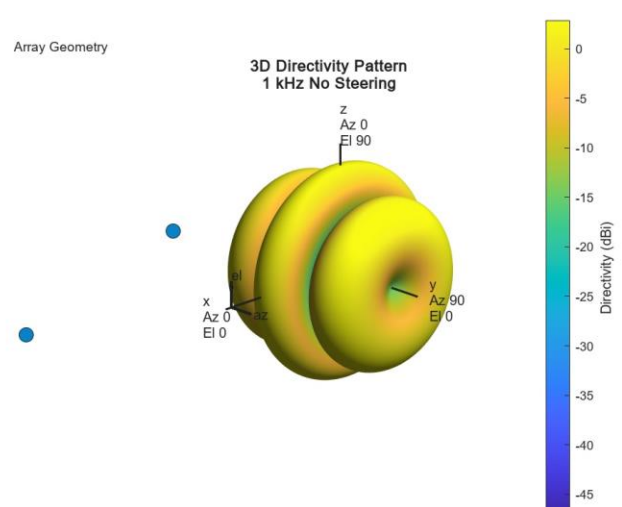
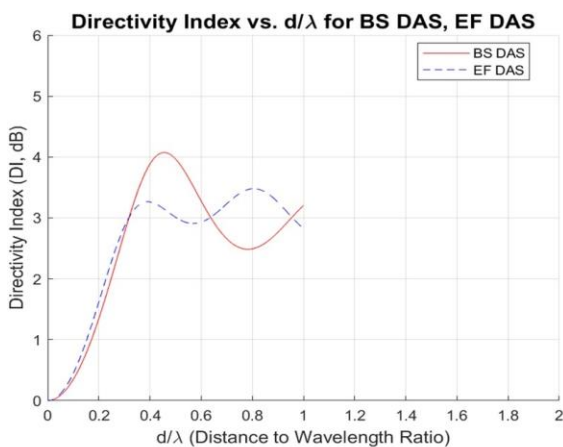


Fig. 7. Directivity index of two-element microphone arrays as a function of the ratio (d/λ) and the 3D directivity pattern

However, the frequency response of microphone arrays with differential algorithms is significantly more uneven than that with delay and summation algorithms. Different efficiency criteria and processing algorithms may be preferable depending on the scenario of the microphone array application. The properties of two-element microphone arrays should be considered when implementing other algorithms for processing the signals of microphone arrays, including algorithms for processing the signals of microphone arrays with many elements.

The degree of directivity of a uniform circular array (UCA) depends on the radius of the circular arrangement of the microphones and the number of elements n . For small radii, the array provides a broad, uniform directivity pattern. As the radius increases, the directivity pattern becomes more focused, and the spatial response develops into multiple lobes. The directivity index (DI) asymptotically approaches the theoretical maximum for DAS algorithms, which depends on the number of array elements and their configuration.

To avoid aliasing and undesirable lobing effects at higher frequencies, the spacing between adjacent microphones along the circumference is limited by the ratio 35, where d represents the arc distance between adjacent microphones.

Cross-microphone arrays are characterized by an orthogonal arrangement of microphones, which improves their spatial resolution and ability to distinguish sounds from different directions. BS-DAS improves the directivity, especially for narrowband signals, but it introduces complexity in real-time applications.

Differential DIF significantly suppresses low-frequency noise. However, its frequency response is une-

ven, which may lead to problems in applications that require constant sensitivity over a wide frequency range.

The uniform circular arrays are designed for 360° coverage, making them ideal for omnidirectional applications. The uniform distribution of microphones around the circle ensures uniform sensitivity in all directions. The DI remained relatively stable, indicating the reliability of the UCA for applications such as conference rooms and video surveillance.

Unlike CMA, UCA has less dependence on d/λ because its symmetry inherently provides high spatial resolution. The DI is stable at lower frequencies; however, as the frequency increases, the spatial resolution improves without significant changes in directivity. Therefore, it is better to use UCA with DAS or EF DAS algorithms for omnidirectional coverage with a balanced frequency response (Fig. 8).

The proposed UCA provides reliable omnidirectional coverage, making it suitable for environments requiring uniform sensitivity.

3. Results and Discussion

In the first stage, the design of the matrix was carried out. To determine the optimal array geometry for sound source localization, the physical and acoustic requirements for the microphone array were first determined based on theoretical analysis. We calculated the acoustic characteristics of the arrays and compared them with respect to their suitability for use in sound localization. We evaluated different methods for calculating the characteristics of microphone arrays, as briefly stated in the theoretical section, where a comparison of results for different microphone array geometries is also given.

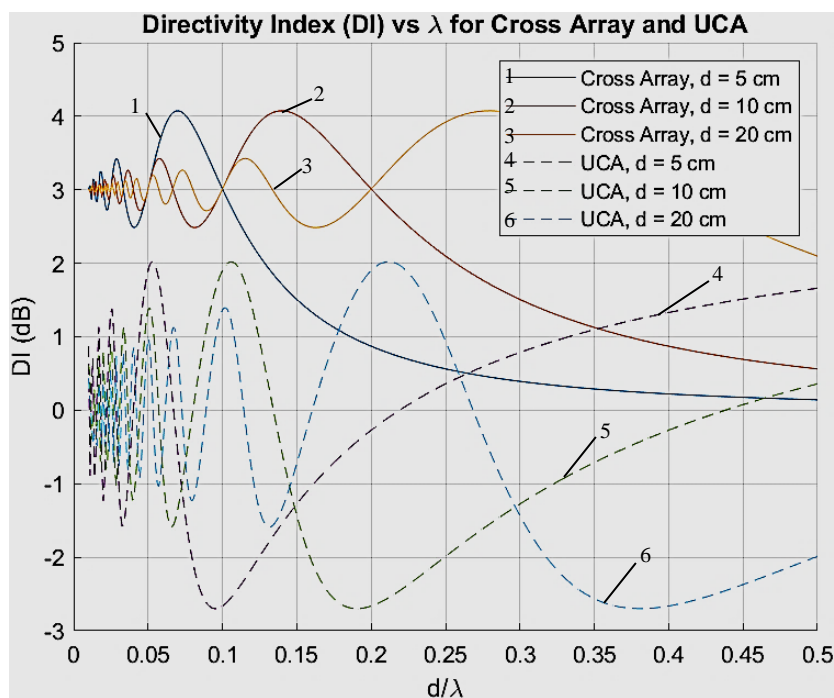


Fig. 8. Directivity index of the cross microphone array and uniform circular array as a function of the ratio (d/λ)

The number of microphones was limited by the cost, available Raspberry Pi 5 inputs, and processing power. The Raspberry Pi board provides I/O ports for 4 I2S microphones. If you use the PCA9548 expansion card, you can connect eight microphones. SPH0645LM4H-B omnidirectional microphones were used (Fig. 9).

For a microphone array to work well for sound localization, the array's beam pattern must have a narrow main lobe and several low-level side lobes in the directivity pattern. These properties depend on the number of microphones and array size. As mentioned earlier, a planar or spherical array with sufficient elements is often used for sound localization, as it provides better spatial resolution and 3D localization capability.

Directivity must have certain minimum values for an array of microphones to be used for sound localization. The array must have a well-defined and high head front for the directional pattern to accurately indicate the direction of the sound source. This is achieved by minimizing the width of the main HPBW. Typically, an HPBW of 30° or less is desirable for most applications.

The side lobes should be at a low level on the directional pattern, ideally not more than -10 dB from the level of the prominent forehead. The SLL should be no more than -20 dB for high-precision sound localization systems. In addition, the directional characteristics should provide uniform sensitivity to sound in different directions.

A uniform planar array (UPA) with a rectangular array of microphones can achieve a narrow main lobe and low side lobes by increasing the number of elements and optimizing their spacing ($d \leq \lambda/2$) can be used to create such an array.

A circular array can also be used because it provides a good balance between directionality and complexity. The circular array can provide a uniform response regarding the azimuth angle with precise directivity and low side lobes.

For a round array with several microphones, four microphones are evenly located around the circle. The angle between the microphones is $\theta = 360/4 = 90^\circ$. Eight are also evenly spaced around the circle. The angle between the microphones is $\theta = 360/8 = 45^\circ$ (Fig. 10).

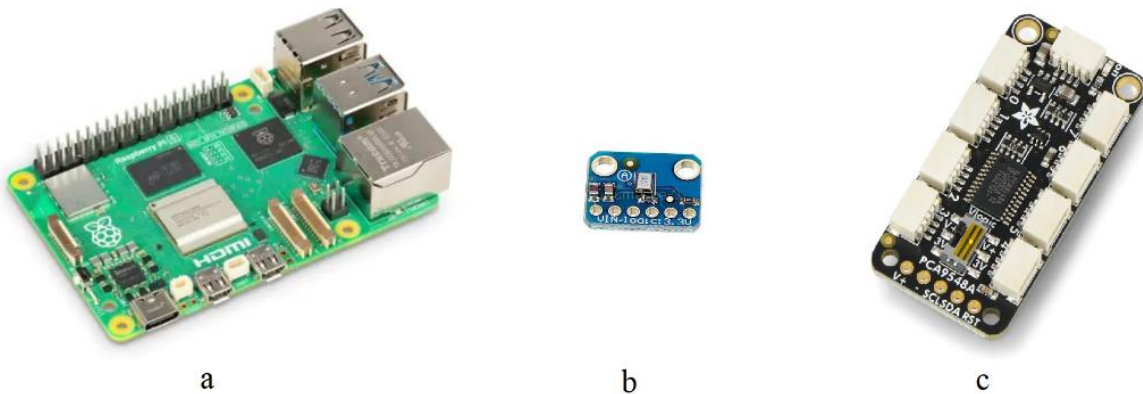


Fig. 9. a) Raspberry Pi 5; b) SPH0645LM4H-B bottom port microphone with an I2S digital output; c) Adafruit PCA9548 8-Channel STEMMA QT

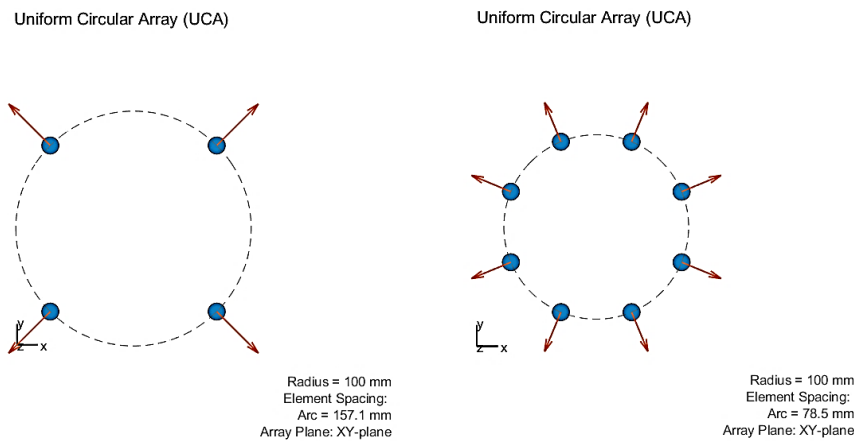


Fig. 10. Circular array configurations for $n = 4$ and $n = 8$

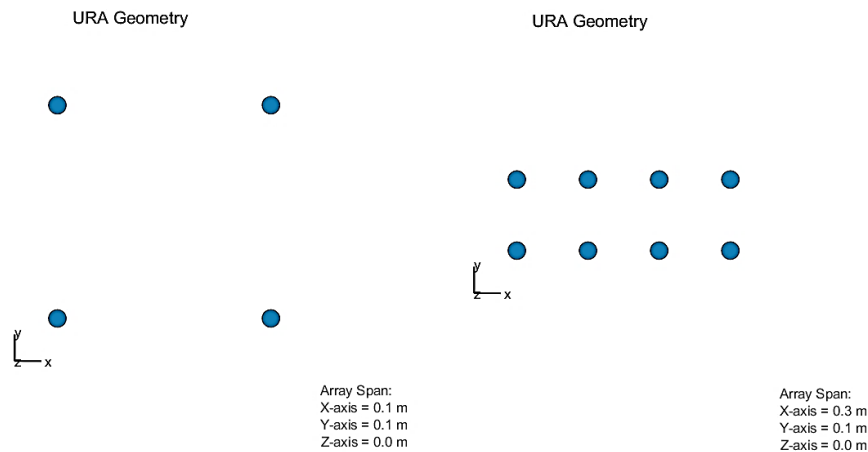


Fig. 11. Uniform rectangle array configurations for $n = 4$ and $n = 8$

The radius of the array can be changed to control its frequency range. A larger radius results in a narrower beam (higher directivity) but requires a higher frequency for effective operation. Higher frequencies provide better sound localization. The radius r is related to the wavelength λ of the sound we need to localize. For example, for sound localization of 1 kHz with a wavelength of $\lambda = c/f$, where $c \approx 343$ m/s is the speed of sound, the wavelength will be $\lambda = 343/1000 = 0.343$ m. For the central petal, the radius r will be from $\lambda/2$ to λ ; we take $r \approx 0.1$ m.

Various geometric microphone array configurations were generated using the Sensor Array Analyzer App in Matlab.

We determined and compared the important characteristics of sound localization for different geometric configurations of microphone arrays.

The Array Directivity is the directional characteristic of the microphone array and is determined at certain angles. For example, the result of the calculation of the array of microphones is 0.84 dBi at 0 Az; 0 El means that the gain level in the direction that coincides with the main beam of the array (at an angle of 0 degrees in azimuth and 0 degrees in elevation) is equal to 0.84 dBi, where the index "i" in dBi indicates the use of an isotropic microphone as a comparison, i.e. the comparison is made with an ideal omnidirectional microphone.

The angular coordinates that determine the position of the sound source in 3D space relative to the centre of the microphone array are Az (azimuth) and El (elevation). The azimuth angle defines the horizontal direction of the sound source relative to the x axis in the xy plane and is measured from the positive x axis in the xy plane counterclockwise. The elevation angle defines the vertical direction of the sound source relative to the horizontal xy plane. It was measured from the xy plane up or down, so the elevation angle is $+90^\circ$ directly above the microphone array. A value of 0 El means that the measurement takes place at the horizon level.

The Array Span represents the array dimensions along three axes, for example, $x = 0$ m; $y = 1.5$ m; and $z = 0$ m.

Number of Elements – the number of microphones in the array.

HPBW (Half Power Beamwidth) is the angular width of an array of microphones or antennas at which the power level is reduced to half the maximum value (or to -3 dB). For example, if the microphone array has $\text{HPBW} = 10^\circ$, the system power will decrease to half the maximum value within an angle of 10° .

FNBW (First Null Beamwidth) is the angular width of the beam between the first null in the beam pattern after the main frontal beam. The distance between two points on the graph where the power level drops to zero indicates signal loss or a complete lack of signal reception. This is a rather important characteristic of the "purity" of the beam, which demonstrates how well the system can isolate signals outside the main beam.

SLL (Side Lobe Level) is the power level of the side lobes of the microphone array's directional pattern compared to the main beam. The value is measured in dB relative to the power level in the main beam. The smaller the SLL, the better the system's ability to concentrate energy in the main beam and reduce side signals (Fig. 12).

Associated with it is the characteristic MSL (Main Sidelobe Level) - the level of the main sidelobe, defined as the difference in levels between the main beam and the most intense sidelobe. Importantly, if the MSL level is high (eg -3dB or more), may indicate significant side lobes, which can degrade system performance due to redundant signals in other directions. The MSL can be calculated using the main parameters of the array directional diagram, in particular, the SLL. First, it is necessary to define the main lobe (Main Lobe) as the directional diagram region containing the gain peak (directivity), usually in the direction of 0° azimuth and 0° elevation.

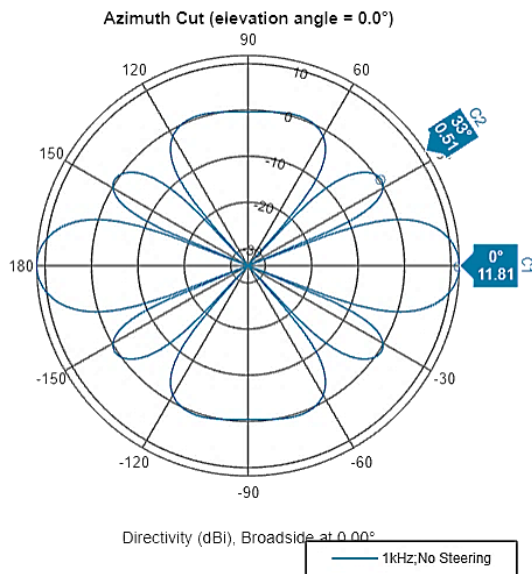


Fig. 12. Azimuth pattern for URA Microphone Arrays with $n = 8$ and $d = 23$ cm. SLL (Side Lobe Level) – the power level of the most prominent side lobe is defined as the difference Array Directivity $11.81 - 0.51 = 11.31$ dB compared to the main beam

MSL can be estimated as

$$\text{MSL} = \text{Peak Gain} - \text{SLL},$$

where Peak Gain – the maximum gain of the main lobe of the array in dB (we obtained it using the Sensor Array Analyzer); SLL is the level of the first side lobe, dB.

Matlab scripts were developed to automate calculations. Here is an example of calculating the Array Directivity of a planar array of four microphones (see Fig. 11):

```
% Create a uniform rectangular array
Array = phased.URA('Size', [2 2], ...
    'Lattice', 'Rectangular', 'ArrayNormal', 'x');
Array.ElementSpacing = [0.23 0.23];
% Calculate taper
rwind = ones(1, 2).';
cwind = ones(1, 2).';
taper = rwind * cwind.';
Array.Taper = taper.';
% Create an omnidirectional microphone element
Elem = phased.OmnidirectionalMicrophoneElement;
Elem.FrequencyRange = [0 6000];
Array.Element = Elem;
% Propagation Speed
PropagationSpeed = 343;
% Frequency range
freqStart = 500;
freqEnd = 6000;
freqStep = 500;
frequencies = freqStart:freqStep:freqEnd;
% Loop through frequencies
for Frequency = frequencies
```

```
% Calculate weights
w = ones(getNumElements(Array), 1);
% Compute pattern
[response, angles] = pattern(Array, Frequency, -180:180, 0, ...
    'PropagationSpeed', PropagationSpeed, ...
    'Type', 'Directivity', 'CoordinateSystem', 'rectangular');
% Peak Gain (Main Lobe)
[PeakGain, peakIdx] = max(response);
% Exclude main lobe for ArrayDirectivity computation
sideLobes = response;
lowerIdx = max(1, peakIdx-5); % Ensure index is within
bounds
upperIdx = min(length(response), peakIdx+5);
sideLobes(lowerIdx:upperIdx) = -Inf; % Mask main lobe
ArrayDirectivity = max(sideLobes); % Side Lobe Level
% Display results for current frequency
disp(['Frequency: ', num2str(Frequency), ' Hz']);
disp([' ArrayDirectivity: ', num2str(ArrayDirectivity), ' dB']);
disp('-----');
end
```

The calculations demonstrate that the geometric configurations of the arrays can be improved for sound localization problems by increasing the distance between the microphones. Therefore, it is necessary to adjust the distance between the microphones to increase the distance between them (reduce the array's radius or the distance between the elements). This approach reduced the beam width; however, limitations due to diffraction at low frequencies must be considered. Doubling the distance for a planar array of 4 microphones resulted in, for example, $\text{HPBW} = 51^\circ$ for a frequency of 1000 Hz. The HPBW must be at least 100° for a frequency of 500 Hz.

The results of calculations of Array Directivity, HPBW, and SLL for each frequency from 500 Hz to 6000 Hz with a step of 500 Hz for four different geometric configurations of microphone arrays (URA $n = 4$ and $n = 8$; USA $n = 4$ and $n = 8$) are shown in the lower tables.

The results show that similar geometric configurations of microphone arrays from omnidirectional microphones can be used for sound localization tasks at low frequencies because they are characterized by good values of Array Directivity and HPBW (Table 6, Table 7). This means creating a sufficiently narrow main beam, where the level of the sidelobe SLL does not differ from that of the main lobe at high frequencies. The best configurations were URA Microphone Arrays with $n = 8$ and $d = 23$ cm (Fig. 13).

It can be seen that the URA Microphone Arrays with $n = 8$ and $d = 23$ cm, based on omnidirectional microphones, can be used for sound localization tasks at low frequencies up to 1000 Hz because the level of the side lobe is lower than the main lobe by about 11 dB, which, if used, can further reduce considered processing algorithms (Table 8, Table 9). At frequencies of 200-300 Hz, there was no side lobe at all, but HPBW was too wide.

Therefore, URA Microphone Arrays were finally

chosen for the project. At this stage, it should be noted that a prototype installation for sound localization can be developed using the selected hardware.

Table 6
Array Directivity, HPBW and SLL
for URA Microphone Arrays with n = 4 and d = 23 cm

Frequency (Hz)	Array Directivity, dBi at 0 Az	HPBW (degrees Az)	SLL (dB Az)
500	3.30	96.24	-
1000	8.78	43.72	5.84
1500	5.75	28.74	0.00
2000	5.42	21.46	0.00
2500	6.58	17.14	0.00
3000	6.17	14.26	0.00
3500	5.40	12.22	0.00
4000	6.72	10.68	0.00
4500	5.81	9.50	0.00
5000	5.84	8.54	0.00
5500	6.24	7.78	0.00
6000	6.08	7.12	0.00

Array Geometry

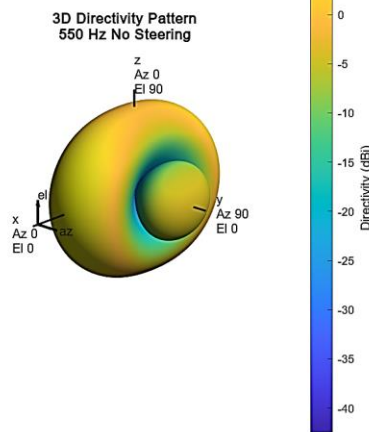


Fig. 13. URA Microphone Arrays with n = 8, d = 23 cm; 3D directivity pattern for 550 Hz. Array Directivity 7.43 dBi at 0 Az; 0 El; HPBW 35.92° Az / 86.00° El; SLL 11.30 dB Az / - dB El

Table 8
Array Directivity, HPBW and SLL
for UCA Microphone Arrays with n = 4 and r = 23 cm

Frequency (Hz)	Array Directivity (dBi)	HPBW (degrees Az)	SLL (dB Az)
500	-15.34	41.34	0.00
1000	5.94	29.66	0.00
1500	-6.79	20.80	0.00
2000	6.29	14.78	0.00
2500	-2.60	12.31	0.00
3000	5.34	10.40	0.00
3500	0.41	8.73	0.00
4000	4.30	7.31	0.00
4500	2.18	6.92	0.00
5000	3.18	5.06	0.00
5500	3.54	5.54	0.00
6000	1.22	5.18	0.00

Table 7
Array Directivity, HPBW and SLL
for URA Microphone Arrays with n = 8 and d = 23 cm

Frequency (Hz)	Array Directivity, dBi at 0 Az	HPBW (degrees Az)	SLL (dB Az)
100	0.38	360	-
200	1.49	115.90	-
500	6.70	39.64	11.95
1000	11.81	19.52	11.30
1500	8.26	12.98	0.00
2000	8.46	9.74	0.00
2500	9.62	7.78	0.00
3000	9.19	6.48	0.00
3500	8.20	5.56	0.00
4000	9.84	4.86	0.00
4500	8.81	4.32	0.00
5000	8.94	3.90	0.00
5500	9.14	3.54	0.00
6000	9.13	3.24	0.00

Table 9
Array Directivity, HPBW and SLL
for UCA Microphone Arrays with n = 8 and r = 35 cm

Frequency (Hz)	Array Directivity (dBi)	HPBW (degrees Az)	SLL (dB Az)
500	-0.71	360.00	-
1000	-10.40	18.60	0.00
1500	6.61	13.12	0.00
2000	3.57	12.06	0.00
2500	-4.99	6.97	0.00
3000	1.92	6.82	0.00
3500	3.29	4.90	0.00
4000	0.91	4.94	0.00
4500	-17.61	5.02	0.00
5000	0.16	4.22	0.00
5500	2.60	3.69	0.00
6000	4.13	3.42	0.00

A low main beam width (HPBW) was achieved to make the microphone array more effective for sound source localization (see Fig. 13). However, the problem of low sidelobe level (SLL) at high frequencies (above 1000 Hz) requires further investigation. This allows for a more accurate determination of the direction of the sound and avoid localization errors that can occur due to high sidelobe levels.

4. Conclusions

Different processing algorithms provide different characteristics for the same microphone array architecture. Differential algorithms make grids more compact and suppress low-frequency noise better than delay and summation algorithms. However, their frequency response was less uniform. Depending on the application, different algorithms and performance criteria may be preferred.

The geometric configuration of microphone arrays significantly affects sound localization performance. By adjusting the distance between the microphones and changing the radius of the array, the directivity of the array and the levels of the side lobes in the directivity pattern can be optimized. Calculations showed that increasing the distance between the microphones improved the beam width reduction. A comparison of different grating configurations, such as uniform rectangular gratings (URA) and uniform circular gratings (UCA), revealed different results for the directivity, half-power beam width (HPBW), and sidelobe levels (SLL). The four-microphone URA configuration showed increased directivity with increasing frequency, with a steady decrease in HPBW, but low sidelobes only at low frequencies (up to 1000 Hz). This study demonstrates the need to find a compromise between array complexity, directivity, and the ability of the system to minimize side lobes on a directivity diagram. Future work must improve array design and apply SSL reduction techniques to improve localization accuracy over a wider frequency range, providing reliable sound localization in real-world applications. The obtained results can be used to develop compact microphone arrays.

Reducing the SLL (level of side lobes) is possible in future studies; it is possible to try to achieve it in various ways, the theoretical bases of which have already been partially developed and covered in the unique literature. In particular, it is possible to single out 1) optimization of the location of elements—search for more complex configuration of arrays; 2) use of phasing, which consists of applying the appropriate phase signal (phasing) to each microphone; 3) use filtering or aperture correction, for example, amplitude weighting (tapering or weighting) allows you to reduce the level of side lobes by changing the weighting coefficients of the array

elements; 4) apply methods to reduce noise. The indicated methods can help reduce the signal intensity in the side lobes.

Future studies should incorporate super-resolution methods for determining the angular position of a radiation source, including the Capon method, which minimizes interference through adaptive beamforming, the thermal noise method, which estimates the signal direction based on noise power variations, the MUSIC algorithm, which employs eigenvalue decomposition for high-resolution spectral estimation, and the ESPRIT algorithm, which leverages signal subspace properties for precise angle estimation.

Contributions of authors: conceptualization, methodology – **Andrii Riabko**; formulation of tasks, analysis – **Oksana Zaika, Roman Kukharchuk**; literature review – **Roman Kukharchuk, Yuriy Smorzhevsky**; development of model, software, verification – **Andrii Riabko, Tetiana Vakaliuk**; analysis of results, visualization – **Andrii Riabko, Tetiana Vakaliuk**; writing – original draft preparation – **Oksana Zaika, Yuriy Smorzhevsky**, writing – review and editing – **Tetiana Vakaliuk**.

Conflict of Interest

The authors declare that they have no conflict of interest related to this research, whether financial, personal, authorship or otherwise, that could affect the research and its results presented in this paper.

Financing

This study was conducted without financial support.

Data Availability

The work has associated data in the data repository.

Use of Artificial Intelligence

The authors used artificial intelligence technologies (Grammarly) within acceptable limits to improve language and readability. After using this tool, they reviewed and edited the content as needed and took full responsibility for the publication's content.

All the authors have read and agreed to the published version of this manuscript.

References

1. Riabko, A., Vakaliuk, T., Zaika, O., Kukharchuk, R., & Kontsedailo, V. Edge computing applications: using a linear MEMS microphone array for UAV position detection through sound source localization. *doors-2024: 4th Edge Computing Workshop*, 2024 vol. 4, pp. 14-36. Available at: <https://ceur-ws.org/Vol-3666/paper02.pdf> (accessed 1.08.2024).

2. Ahlefeldt, T., Haxter, S., Spehr, C., Ernst, D., & Kleindienst, T. Road to acquisition: Preparing a MEMS microphone array for measurement of fuselage surface pressure fluctuations. *Micromachines*, 2021, no 12, iss. 8, article no. 961. DOI: 10.3390/mi12080961.
3. Dela Cruz, J. C., Dela Cueva, E. P. P., Labrador, D. F. L., & Ibera, J. Digital MEMS Beamforming Microphone Array for Small-scale Video Conferencing, *IEEE 9th Conference on Systems, Process and Control*, 2021, pp. 162-167. DOI: 10.1109/ICSPC53359.2021.9689108.
4. Liu, H., Barekatin, M., Roy, A., Liu, S., Cao, Y., Tang, Y., & Kim, E. S. MEMS piezoelectric resonant microphone array for lung sound classification. *Journal of Micromechanics and Microengineering*, 2023, vol. 33, iss. 4. DOI: 10.1088/1361-6439/acbf3.
5. Leman, R., Travaglione, B., & Hodkiewicz, M. Beamforming using Digital Piezoelectric MEMS Microphone Array. *arXiv preprint arXiv:2111.100873031*, 2021. DOI: 10.48550/arXiv.2111.10087.
6. Adorno, S., Cerini, F., & Vercesi, F. Microphones. In: Vigna, B., Ferrari, P., Villa, F.F., Lasalandra, E., & Zerbini, S. (eds) *Silicon Sensors and Actuators*. Springer, 2022, pp. 503-522. DOI: 10.1007/978-3-030-80135-9_15.
7. Kumar, A., Varghese, A., Kalra, D., Raunak, A., Prasad, M., Janyani, V., & Yadav, R. P. MEMS-based piezoresistive and capacitive microphones: A review on materials and methods. *Materials Science in Semiconductor Processing*, 2024, vol. 169, article no. 107879. DOI: 10.1016/j.mssp.2023.107879.
8. Izquierdo, A., Val, L. D., & Villacorta, J. J. Feasibility of using a MEMS microphone array for pedestrian detection in an autonomous emergency braking system. *Sensors*, 2021, vol. 21, iss. 12, article no. 4162. DOI: 10.3390/s21124162
9. Kumar, A., Varghese, A., Sharma, A., Prasad, M., Janyani, V., Yadav, R. P., & Elgaid, K. Recent development and futuristic applications of MEMS-based piezoelectric microphones. *Sensors and Actuators A: Physical*, 2024, vol. 347, article no. 113887. DOI: 10.1016/j.sna.2022.113887.
10. Yan, J., Chen, C., Wu, Z., Ding, X., & Lou, L. An acoustic localisation sensor based on MEMS microphone array for partial discharge. *Sensors*, 2023, vol. 23, iss. 3, article no. 1077. DOI: 10.3390/s23031077.
11. Laurijssen, D., Daems, W., & Steckel, J. Broadband MEMS Microphone Arrays with Reduced Aperture Through 3D-Printed Waveguides. *arXiv preprint arXiv:2406.0766*, 2023. DOI: 10.48550/arXiv.2406.07663.
12. Verreycken, E., Simon, R., Quirk-Royal, B., Daems, W., Barber, J., & Steckel, J. Bio-acoustic tracking and localisation using heterogeneous, scalable microphone arrays. *Communications Biology*, 2021, vol. 4, iss. 1, article no. 1275. DOI: 10.1038/s42003-021-02746-2.
13. Daniel, E., Geisler, R., Philipp, F., Ahlefeldt, T., Goudarzi, A., & Carsten, S. Enhancing aeroacoustic wind tunnel studies through massive channel upscaling with MEMS microphones. *30th AIAA/CEAS Aeroacoustics Conference*, June 4-7, 2024, Rome, Italy. DOI: 10.2514/6.2024-3064.
14. Duanmu, Z., Kong, C., Guo, Y., Zhang, X., Liu, H., Zhao, C., & Wan, C. Design and implementation of an acoustic-vibration capacitive MEMS microphone. *AIP Advances*, 2022, vol. 12, iss. 6. DOI: 10.1063/5.0090687.
15. Chang, E. T., Wang, R., Ballentine, P., Xu, J., Smith, T., Coltin, B., & Ciocarlie, M. An investigation of multi-feature extraction and super-resolution with fast microphone arrays. *IEEE International Conference on Robotics and Automation (ICRA)*, Yokohama, Japan, 2024, pp. 3388-3394. DOI: 10.1109/ICRA57147.2024.10611599.
16. Pecioski, D., Markovska, S. D., Gavriloski, V., Anachkova, M., & Ignjatovska, A. Development of low-cost MEMS microphone array for sound localisation in urban environments. *INTER-NOISE and NOISE-CON Congress and Conference Proceedings*, 2024, vol. 270, iss. 7, pp. 4641-4651. DOI: 10.3397/IN_2024_3490.
17. Wu, L., Chen, X., Ngo, H. D., Julliard, E., & Spehr, C. Design of dual-frequency piezoelectric MEMS microphones for wind tunnel testing. *AIAA SciTech 2022 Forum*, 2022, article no. 1021. DOI: 10.2514/6.2022-1021.
18. Cheng, C. Y., Saputra, I., Lin, C. W., & En, S. C. Development of Dynamic Platform with MEMS Microphones Array Embedded for UAV Detection and Tracking. *International Conference on Consumer Electronics-Taiwan (ICCE-Taiwan)*, 2024, pp. 73-74. DOI: 10.1109/ICCE-Taiwan62264.2024.10674652.
19. Le Son, P. Irregular microphone array design for broadband beamforming. *Signal Processing*, 2022, vol. 193, article no. 108431. DOI: 10.1016/j.sigpro.2021.108431.
20. Li, L., Wang, L., Dong, J., Fu, J., Gao, Y., Qiao, Y., & Zhu, M. SuperSoundcompass: a high-accuracy acoustic localisation sensor using a small-aperture microphone array. *Measurement Science and Technology*, 2023, vol. 32, iss. 10, article no. 105106. DOI: 10.1088/1361-6501/ac0009.
21. Wijnings, P. W., Stuijk, S., Scholte, R., & Corporaal, H. Characterisation of MEMS microphone sensitivity and phase distributions with applications in array processing. *ICASSP 2021-2021 IEEE International Conference on Acoustics, Speech and Signal Processing (ICASSP)*, 2021, pp. 4480-4484. DOI: 10.1109/ICASSP39728.2021.9413352.

Received 17.01.2025, Accepted 17.02.2025

**ПОРІВНЯЛЬНИЙ АНАЛІЗ ТА ВИБІР ГЕОМЕТРИЧНОЇ КОНФІГУРАЦІЇ
МІКРОФОННОГО МАСИВУ НА ОСНОВІ MEMS-МІКРОФОНІВ
ДЛЯ ЗАДАЧ ЛОКАЛІЗАЦІЇ ЗВУКУ**

**А. В. Рябко, Т. А. Вакалюк, О. В. Заїка,
Р. П. Кухарчук, Ю. Л. Сморжевський**

Предметом вивчення є розробка геометричної конфігурації масиву всенаправлених MEMS-мікрофонів для задач локалізації звуку. **Метою** є створення компактних і високоточних пристроїв для локалізації звуку, які забезпечують збалансоване всенаправлене покриття та точність роботи в широкому частотному діапазоні. **Завдання** дослідження включають аналіз просторово-частотних характеристик різних архітектур мікрофонних решіток (лінійний масив, плоский масив, коловий масив, концентричний масив) і порівняння алгоритмів формування променів для задач локалізації (затримково-сумовий, диференціальний, наднаправлений формувачі променю). **Методи** дослідження базуються на застосуванні як відомих, так і авторських аналітичних моделей для передатних функцій і коефіцієнтів спрямованості, а також експериментальній перевірці прототипу пристрою на основі апаратної платформи Raspberry Pi 5 з платою розширення Adafruit PCA9548 8-Channel STEMMА QT та всенаправленими MEMS-мікрофонами SPH0645LM4H-B. **Результати** дослідження показали, що диференціальні алгоритми мають перевагу перед алгоритмами затримки та підсумовування при виділенні цільових сигналів в умовах ізотропного шумового поля і когерентних джерел шуму. Оптимальною геометрією для збалансованого всенаправленого покриття є UCA з алгоритмами DAS або EF DAS, які забезпечують хорошу спрямованість і низькі рівні бічних пелюсток. Найпростіша та ефективна чотиримікрофонна конфігурація URA покращує спрямованість із збільшенням частоти, але низькі бічні пелюстки досягаються лише на частотах до 1000 Гц. **Висновки.** Геометрична конфігурація мікрофонних масивів та алгоритми формування променів є критично важливими для ефективною локалізації звуку. Подальші дослідження будуть спрямовані на вдосконалення масивів за допомогою методів редукції SSL для покращення точності локалізації в широкому частотному діапазоні. Отримані результати можуть бути використані для розробки компактних і високоефективних мікрофонних масивів.

Ключові слова: локалізація джерела звуку; мікрофон MEMS; мікрофонний масив; спрямованість; рівень бічних пелюсток.

Рябко Андрій Вікторович – канд. пед. наук, доц. каф. фіз.-мат. освіти та інформатики, Глухівський національний педагогічний університет імені Олександра Довженка, Глухів, Україна.

Вакалюк Тетяна Анатоліївна – д-р пед. наук, проф., зав. каф. інженерії програмного забезпечення, Державний університет «Житомирська політехніка», Житомир, Україна.

Заїка Оксана Володимирівна – канд. пед. наук, доц. каф. фіз.-мат. освіти та інформатики, Глухівський національний педагогічний університет імені Олександра Довженка, Глухів, Україна.

Кухарчук Роман Павлович – канд. пед. наук, доц., зав. каф. фіз.-мат. освіти та інформатики, Глухівський національний педагогічний університет імені Олександра Довженка, Глухів, Україна.

Сморжевський Юрій Людвігович – канд. пед. наук, доц., зав. каф. математики, Кам'янець-Подільський національний університет імені Івана Огієнка, Кам'янець-Подільський, Україна.

Andrii Riabko – Candidate of Pedagogical Sciences, Associate Professor at the Department of Physical and Mathematical Education and Informatics, Oleksandr Dovzhenko Hlukhiv National Pedagogical University, Ukraine, e-mail: ryabko@meta.ua, ORCID: 0000-0001-7728-6498, Scopus Author ID: 57225896687.

Tetiana Vakaliuk – Doctor of Pedagogical Sciences, Professor, Head of the Department of Software Engineering, Zhytomyr Polytechnic State University, Zhytomyr, Ukraine, e-mail: tetianavakaliuk@gmail.com, ORCID: 0000-0001-6825-4697, Scopus Author ID: 57211133927.

Oksana Zaika – Candidate of Pedagogical Sciences, Associate Professor at the Department of Physical and Mathematical Education and Informatics, Oleksandr Dovzhenko Hlukhiv National Pedagogical University, Ukraine, e-mail: ksuwazaika@gmail.com, ORCID: 0000-0002-8479-9408, Scopus Author ID: 57223102528.

Roman Kukharchuk – Candidate of Pedagogical Sciences, Associate Professor, Head of the Department of Physical and Mathematical Education and Informatics, Oleksandr Dovzhenko Hlukhiv National Pedagogical University, Ukraine, e-mail: kuxap4yk1@ukr.net, ORCID: 0000-0002-7588-7406, Scopus Author ID: 57223104682.

Yuriy Smorzhevsky – Candidate of Pedagogical Sciences, Associate Professor, Head of the Department of Mathematics, Kamianets-Podilskyi Ivan Ohienko National University, Kamianets-Podilskyi, Ukraine, e-mail: smorzhevskyi@kpnu.edu.ua, ORCID: 0000-0001-9832-3390.